ORIGINAL ARTICLE

Global, Low-Amplitude Cortical State Predicts Response Outcomes in a Selective Detection Task in Mice

Krista Marrero[1,†], Krithiga Aruljothi[2,†], Behzad Zareian[2], Chengchun Gao[3], Zhaoran Zhang [1] and Edward Zagha[1,2]

[1]Neuroscience Graduate Program, University of California Riverside, Riverside, CA 92521, USA, [2]Department of Psychology, University of California Riverside, Riverside, CA 92521, USA and [3]Department of Bioengineering, University of California Riverside, Riverside, CA 92521, USA

Address correspondence to Edward Zagha. Email: edward.zagha@ucr.edu
[†]Krista Marrero and Krithiga Aruljothi have contributed equally to this work.

Abstract

Spontaneous neuronal activity strongly impacts stimulus encoding and behavioral responses. We sought to determine the effects of neocortical prestimulus activity on stimulus detection. We trained mice in a selective whisker detection task, in which they learned to respond (lick) to target stimuli in one whisker field and ignore distractor stimuli in the contralateral whisker field. During expert task performance, we used widefield Ca^{2+} imaging to assess prestimulus and post-stimulus neuronal activity broadly across frontal and parietal cortices. We found that lower prestimulus activity correlated with enhanced stimulus detection: lower prestimulus activity predicted response versus no response outcomes and faster reaction times. The activity predictive of trial outcome was distributed through dorsal neocortex, rather than being restricted to whisker or licking regions. Using principal component analysis, we demonstrate that response trials are associated with a distinct and less variable prestimulus neuronal subspace. For single units, prestimulus choice probability was weak yet distributed broadly, with lower than chance choice probability correlating with stronger sensory and motor encoding. These findings support low amplitude and low variability as an optimal prestimulus cortical state for stimulus detection that presents globally and predicts response outcomes for both target and distractor stimuli.

Key words: choice probability, neocortex, prestimulus, sensory detection, widefield imaging

Introduction

The brain is never silent. Throughout sleep and wakefulness, spontaneous neuronal activity reflects dynamic, self-organized states that affect the generation and propagation of neuronal signals (Arieli et al. 1995, 1996; Ferezou et al. 2007; Niell and Stryker 2010; Poulet et al. 2012; Palmer et al. 2014; Zagha and McCormick 2014; McCormick et al. 2015; McGinley, David, et al. 2015a; McGinley, Vinck, et al. 2015b). Changes in spontaneous activity impact the amplitude of neuronal sensory responses (Sachdev et al. 2004; Crochet and Petersen 2006; Poulet and Petersen 2008; Haider and McCormick 2009;

Shimaoka et al. 2018) and behavioral outcomes (Boly et al. 2007; Mazaheri et al. 2011; McGinley, David, et al. 2015a; van Kempen et al. 2020; Fiebelkorn and Kastner 2021; Kim and Sejnowski 2021). In awake subjects, these changes correlate with changes in task engagement, movement, and internal (cognitive or egocentric) versus external (perceptive or allocentric) processing modes (Boly et al. 2007; de Lange et al. 2013; Murphy et al. 2018; Stringer et al. 2019; Andreou and Borgwardt 2020; Musall et al. 2020; Salkoff et al. 2020). However, most studies of sensory processing and sensory detection normalize post-stimulus by prestimulus activity, thereby obscuring the impacts of

spontaneous activity. And yet, understanding how spontaneous activity impacts neuronal signaling and task performance will reveal important principles of context-dependent sensory and motor processing.

This study focuses on prestimulus activity during a sensory detection task in mice for which many open questions remain. First is the ability to detect a stimulus improved by high or low prestimulus activity (Fig. 1A)? A common model of decision-making is integration to bound, which proposes that a decision is made once neuronal activity reaches a specific threshold (Hanes and Schall 1996; Roitman and Shadlen 2002; Gold and Shadlen 2007). Within this model, higher prestimulus activity may bring a network closer to decision threshold and/or increase the gain of a network and therefore promote stimulus detection (Haider and McCormick 2009). Consistent with this framework, studies in primary visual cortex demonstrate that higher prestimulus activity leads to larger amplitude stimulus responses (Haider et al. 2007). However, higher prestimulus activity may reduce cortical stimulus responses (Hasenstaub et al. 2007), due to increased cortical inhibition and reduced intrinsic and synaptic excitability. Studies in the primary somatosensory and primary auditory cortices support this alternative noise suppression framework, demonstrating that lower prestimulus activity, or activity in a low-arousal synchronized state, leads to larger amplitude stimulus responses (Petersen et al. 2003; Sachdev et al. 2004; McGinley, David, et al. 2015a).

In somatosensory (whisker) detection tasks, impacts of prestimulus activity on stimulus encoding and detection have been studied at the level of membrane potential through whole cell patch clamp recordings. While prestimulus membrane potential activity of primary somatosensory cortical neurons did predict sensory response amplitudes (Sachidhanandam et al. 2013), it did not predict trial outcome (e.g., hit vs. miss) (Sachidhanandam et al. 2013; Yang et al. 2016). However, these whole cell recording studies are limited by relatively small samples sizes (10s of neurons), which may obscure the ability to resolve small yet widespread contributions of prestimulus activity to task performance.

A second open question is whether the prestimulus activity that impacts stimulus encoding and detection is focal and restricted to specific cortical regions or global and observed throughout neocortex (Fig. 1B). Global activity may reflect changes in arousal and movement (Stringer et al. 2019; Musall et al. 2020; Salkoff et al. 2020), whereas focal changes may reflect shifts in, for example, attentional focus or response preparation (Luck et al. 1997; Fries et al. 2001; Ghose and Maunsell 2002; Moore and Armstrong 2003). It is currently unknown whether prestimulus activity in sensory compared to motor cortices have larger impacts on task performance, and whether the directionality of that impact is the same across neocortical regions (Shimaoka et al. 2018). In addition to considering different cortices individually, is there an "optimal state" of prestimulus activity that includes the contributions of multiple cortices (Fig. 1C)? A third open question is whether prestimulus activity has the same or different impacts on target (attended) versus distractor (unattended) stimulus encoding and detection (Fig. 1A,C). For example, the same prestimulus activity may promote discrimination (response to targets, no response to distractors) or bias responses for detection (respond to or ignore all stimuli). Finally, do the neurons that express task-relevant changes in prestimulus activity overlap with or are they distinct from the neuronal populations that express strong post-stimulus sensory and/or motor activity (Fig. 1D)?

We address these questions in the context of a selective whisker detection task in mice. We trained mice to respond (lick) to deflections on one whisker field (target) and ignore deflections in the contralateral whisker field (distractor) (Aruljothi et al. 2020; Zareian et al. 2021). Using widefield Ca^{2+} imaging, we previously identified the cortical regions that are highly active post-stimulus and pre-response, and therefore may contribute to stimulus detection: the whisker region of primary somatosensory cortex (wS1), the whisker region of primary motor cortex (wMC), and the pre-motor licking region anterior lateral motor cortex (ALM) (Aruljothi et al. 2020). We consider these cortical regions to be "task-related" and all other cortical regions to be "task-unrelated". Here, we implement a sliding window normalization to preserve prestimulus fluctuations. We investigate the impacts of prestimulus activity levels on trial outcome, for both target and distractor stimuli. Additionally, we use dimensionality reduction of the imaging data to assess prestimulus variability across cortices. Lastly, we assess prestimulus choice probability of single units in task-related cortices to determine the distribution of these signals across the neuronal population.

Methods

The experimental datasets in this study were previously published, including the whisker monitoring, widefield GCaMP6 imaging (Aruljothi et al. 2020) and single unit recordings (Zareian et al. 2021). Below, we summarize these experimental methods and describe the new analyses used in this study.

Animal Subjects

Experiments were approved by the IACUC of University of California, Riverside. Both male and female adult mice were used, either wild type (C57BL/6J, BALB/cByJ) or transgenic (Snap25-2A-GCaMP6s-D, backcrossed to BALB/cByJ). GCaMP6s expressing transgenic mice were used for widefield Ca^{2+} imaging; wild-type mice were used for whisker imaging and electrophysiology. Mice were housed in a 12-h light/dark cycle; experiments were conducted during the light cycle.

Animal Surgery

For headpost implantation, mice were placed under isoflurane (1–2%), ketamine (100 mg/kg), and xylazine (10 mg/kg) anesthesia. The scalp was cut (10 × 10 mm) and resected to expose the skull. A lightweight metal headpost was fixed onto the skull using cyanoacrylate glue. An 8 × 8 mm headpost window exposed most of dorsal cortex. The skull was covered with a thin layer of cyanoacrylate gap-filling medium (Insta-Cure, Bob Smith Industries) to seal the exposed skull and enhance skull transparency; the window was sealed with a quick-dry silicone gel (Reynolds Advanced Materials). Mice were administered meloxicam (0.3 mg/kg) and enrofloxacin (5 mg/kg) for 3 days post-op. Water restriction began after recovery from surgery (minimum of 3 days). Training on the behavior rig began after one day of water restriction. For electrophysiological recordings, craniotomies, and durotomies (<0.5 mm diameter) were performed under isoflurane anesthesia. Full recovery from anesthesia was allowed (up to 60 min) before placement on the behavioral rig.
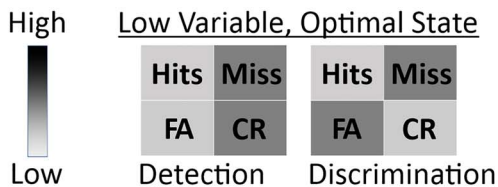
Animal Behavior

Training stages, metrics of learning, and criterion for expert performance in the Go/NoGo selective whisker detection task were
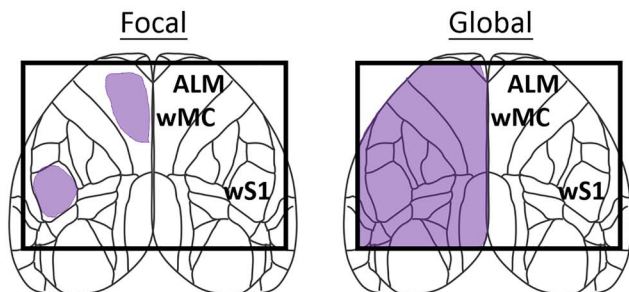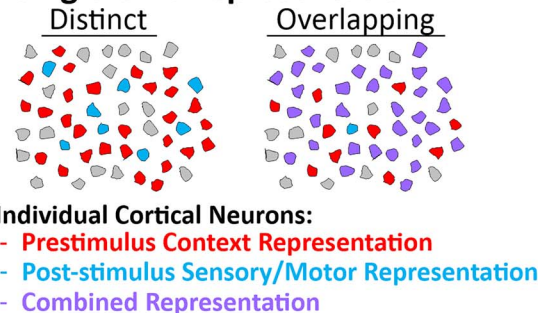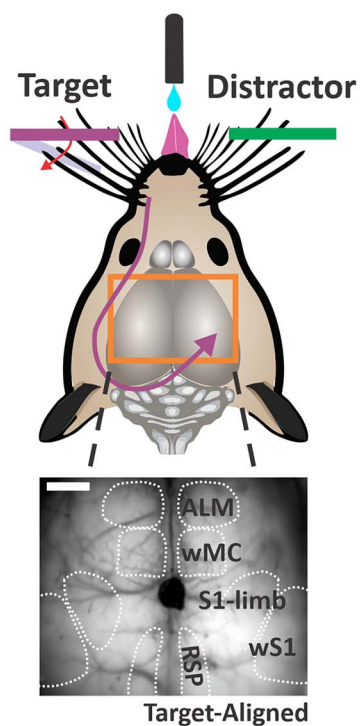
A Function of Neural *Activity*

High Decision Threshold   Noise Suppression

Hits	Miss
FA	CR

Hits	Miss
FA	CR

Hits	Miss
FA	CR

Low

Detection   Discrimination

C Function of Neural *Variance*

High Low Variable, Optimal State

Hits	Miss
FA	CR

Hits	Miss
FA	CR

Low

Detection   Discrimination

B *Focal* or *Global* Effects

Focal   Global

ALM
wMC
wS1

ALM
wMC
wS1

D Single Unit Representation

Distinct   Overlapping

Individual Cortical Neurons:
- **Prestimulus Context Representation**
- **Post-stimulus Sensory/Motor Representation**
- **Combined Representation**

E

Target   **Distractor**

ALM
wMC
S1-limb
wS1
RSP

Target-Aligned

F

	Response	**No Response**
Target Stimulus	Hit 💧	Miss
Distractor Stimulus	False Alarm	Correct Rejection
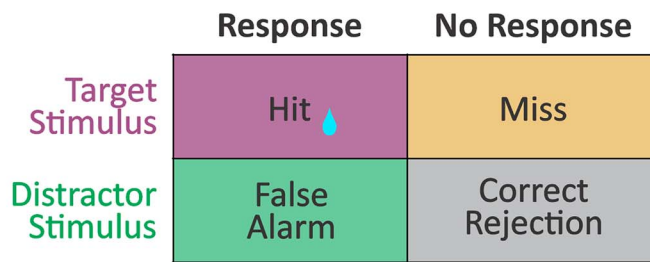
$$d' = z_{Hit\ Rate} - z_{False\ Alarm\ Rate}$$

G

Stimulus

Target → Hit 💧 / Miss
Distractor → FA / CR
Stimulus → Preme
No Stimulus → Spont

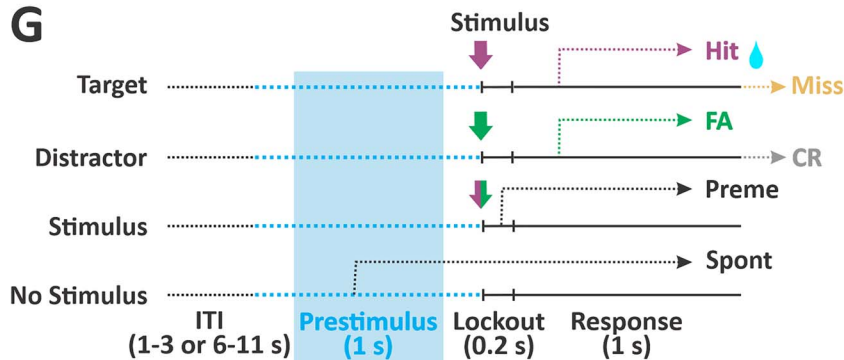| ITI (1-3 or 6-11 s) | Prestimulus (1 s) | Lockout (0.2 s) | Response (1 s) |

Figure 1. Predictions and experimental design for testing impacts of prestimulus activity on sensory detection and discrimination. (*A–D*) Potential mechanisms of task-relevant prestimulus activity. (*E–G*) Experimental design. (*E*) Head-fixed mice are trained to discriminate between target whisker deflections (purple) and distractor whisker deflections (green), within opposite whisker fields. Mice report detection by licking a central lickport. The orange rectangle reflects the widefield Ca^{2+} imaging window. The inset below is a sample imaging frame, demarcating neocortical regions of interest in bilateral frontal and parietal cortices. (*F*) Classification of trial types and outcomes. Task performance is quantified by discrimination d' as the separation between hit and false alarm rates. z, inverse cumulative function of the normal distribution. (*G*) Trial structure, including a variable inter-trial interval, 1-s prestimulus window, 0.2-s stimulus and lockout (delay) window, and 1-s response window. The prestimulus window of interest in this study is the last 1 s of the inter-trial interval (blue shade), immediately before stimulus onset. Spont, spontaneous responses during the prestimulus window; Preme, premature responses during the lockout window. Scale bar in (*E*) is 1 mm.

previously reported (Aruljothi et al. 2020). Briefly, head-fixed and water deprived mice were placed on a behavioral apparatus controlled by Arduino and custom MATLAB (MathWorks) scripts. Two paddles were placed in whisker fields on the opposite sides of the face, designated as target or distractor. Target and distractor designations were assigned at the beginning of training and remained constant. Following variable intertrial intervals, mice could receive a target trial (rapid deflection of the target paddle), distractor trial (rapid deflection of the distractor paddle) or catch trial (no whisker stimulus). Mice responded by

licking at a central lick port. Hits (responses to target stimuli) were rewarded with ~5 μL of water, correct rejections (not responding to distractor stimuli) and correct withholdings (not responding during the catch trial) were rewarded with a shortened intertrial-interval (ITI) and a subsequent target trial. Licking during the ITI was punished by resetting the ITI, effectively a time-out. Mice were considered expert once they achieved a discriminability $d' > 1$ (separation of hit and false alarm response rates) for three consecutive days:

$$\text{discriminability } d' = \phi_{\text{Hit rate}}^{-1} - \phi_{\text{False alarm rate}}^{-1}$$

All recordings were conducted in expert mice while performing the task.

Widefield Imaging

Widefield imaging during expert task performance was conducted as previously reported. The dataset consists of 38 behavioral/imaging sessions, recorded from five mice. The through-skull imaging window included bilateral dorsal parietal and frontal cortices. Illumination from a 470 nm LED source (Thorlabs) was band-pass filtered for excitation (Chroma ET480/40×) and directed onto the skull via a dichroic mirror (Chroma T510lpxrxt). Emitted fluorescence was band-pass filtered (Chroma ET535/50 m) and collected using an RT sCMOS camera (Diagnostic Imaging, SPOT Imaging software). Images were acquired at 10 Hz with a final resolution of 142 × 170 pixels (41 μm per pixel). Image sequences were imported to MATLAB for subsequent analyses.

Electrophysiology

Single unit recordings during expert task performance were conducted as previously reported (Zareian et al. 2021). The dataset consists of 32 behavioral/recording sessions, recorded from 22 mice, yielding a total of 936 single units from three cortical regions (target-aligned whisker region of primary somatosensory cortex [wS1], whisker region of motor cortex [wMC], and anterior lateral motor cortex [ALM]). Coordinates (mm, from bregma): wS1 3.2–3.7 lateral, 1–1.5 posterior; wMC 0.5–1.5 lateral, 1–2 anterior; ALM 1–2 lateral, 2–2.5 anterior. Recordings were targeted to layer 5 of wS1, wMC, and ALM, approximately 500–1100 μm below the pial surface. Electrophysiological recordings were conducted using a silicon multielectrode probe (NeuroNexus A1x16-Poly2-5 mm-50s-177), positioned using a Narishige micro-manipulator. Neuralynx amplifier (DL 4SX 32ch System) and software were used for data acquisition and spike sorting.

Whisker Imaging

Whisker imaging during expert task performance was conducted as previously reported (Aruljothi et al. 2020). The dataset consists of nine behavioral/recording sessions, recorded from four mice. Images were acquired with a CMOS Camera (Thorlabs DCC3240M camera with Edmund Optics lens 33–301) at either 20 or 60 Hz. No systematic difference between 20 and 60 Hz was observed (data not presented). The imaging field of view included both paddles and the mouse's head (including whiskers and snout).

Data Analysis

Data analyses were performed in MATLAB using custom scripts.

Engagement Period

To ensure that analyses were conducted during task engagement, "engaged periods" were defined as continuous behavioral performance of at least 10 min without 60 s of no responding. For sessions with more than one engaged period, the longest engaged period was used for further analyses. Furthermore, sessions were included in subsequent analyses only if performance was at expert level: discriminability $d' > 1$. For sessions with multiple stimulus amplitudes, trials were combined for further analyses only when the differences in response rates were 15% or less.

Sliding Window Normalization and Trial-Based Neuronal Activity

The trial-based imaging time window consisted of the prestimulus epoch (1 s), the stimulus and lockout epoch (0.2 s), and the allowable response epoch (1 s), a total of 2.2 s. A raw movie F was created by concatenating fluorescence activity from consecutive trials, where $F_n(i,j,f)$ is the fluorescence of each pixel (row i and column j) in frame f for each trial n. To generate normalized fluorescence values, we first determined the sliding window local mean for each pixel, computed every 2 s using a ±200-s window size [$F_{\text{SW}}(i,j,n)$]. Then, we calculated the normalized fluorescence (Salkoff et al. 2020) (see also Supplementary Fig. 1) for each pixel at each frame as:

$$\text{d}F_{\text{SW}}/F_{\text{SW}}(i,j,n) = [F_n(i,j,f) - F_{\text{SW}}(i,j,n)]/F_{\text{SW}}(i,j,n)$$

Trialwise average movies were then compiled by first indexing outcome type ("hit, miss, false alarm, correct rejection") and then by averaging pixelwise activity across corresponding frames of corresponding trials. Frames were temporally aligned to the stimulus onset frame (stimulus-aligned) where stimulus occurred or aligned to the first frame containing the response (response-aligned) where response occurred. Trials with responses during the lockout period were considered "premature" and excluded from the analysis. Trials with responses before the stimulus but within the prestimulus imaging period were considered "spontaneous", dF/F reported but not further analyzed. Grand average movies ($n = 38$ sessions) were spatially aligned to bregma, flipped at bregma according to target-distractor assignment, and then averaged across all sessions. Trialwise average, standard deviations (SD), and differences in averages and standard deviations were compiled and aligned as above, but across the full 1 s prestimulus epoch ($n = 38$ sessions).

Difference in Prestimulus Fluorescence

Fluorescence differences for target and distractor assignment were calculated per trial type per session. Prestimulus frames 6–10 (capturing the last 500 ms of the prestimulus window, before stimulus onset) were trialwise and pixelwise averaged per session. Session data were excluded from this analysis if there were fewer than five incorrect trials in the session (excluding nine sessions for target Miss, six sessions for distractor FA). For target fluorescence difference frames ($n = 29$ sessions),

Hits fluorescence mean frame was subtracted from Miss fluorescence mean frame. For distractor fluorescence difference frames ($n = 32$ sessions), FA fluorescence mean frame was subtracted from CR fluorescence mean frame. Response prestimulus frames were subtracted from no response prestimulus frames because no response fluorescence activity was generally higher than response fluorescence activity. Prestimulus difference frames were aligned, assigned, and averaged across all sessions (as above). To normalize for differences in changes in fluorescence across regions, we indexed the pixelwise mean of fluorescence map differences across sessions normalized by the pixelwise deviation in fluorescence map differences across sessions ($\mu_{i,j}/\sigma_{i,j}$). For quantification of target versus distractor prestimulus difference, normalized difference (index), and significance, frames were averaged across pixels for scalar values.

Regression Analyses between Prestimulus Activity and Reaction Time for Response Trials

The correlation between activity during prestimulus period (dF/F) and reaction times (RT) for response trials (Hits and FAs) were computed as a linear regression from which we obtained the slope of the linear fit with 95% confidence interval and coefficient of determination, R^2, as the goodness of fit (Zareian et al. 2020) (Curve Fitting Toolbox in Matlab). For this analysis, we assigned prestimulus dF/F as the independent variable and reaction time as the dependent variable.

Defining Cortical Regions of Interest

For task relevant and task irrelevant cortical regions, we defined a center pixel according to pixel resolution (41 μm) and alignment with bregma as center pixel value = [coordinates from bregma (in mm)]/0.041 mm. Thus, we converted coordinates from bregma (mm) [wS1 ± 3.4 lateral, 1.2 posterior; wMC ± 1.2 lateral, 1.2 anterior; ALM ± 1.5 lateral, 2.3 anterior; RSP ± 0.4 lateral, 2.4 posterior; limb S1 ± 2.0 lateral, 0.6 posterior] to coordinates from bregma (pixels); we then systematically defined rectangles about the center pixel with width (±medial/lateral) and height (±anterior/±posterior) in pixels [wS1 10, 25; wMC 15, 15; ALM 15, 15; RSP 10, 25; limb S1 25, 25]. Rectangles that fell off-frame were cropped at frame borders instead of shifted. Subsequent analyses for region specific Hits-Miss, dF/F versus RT, and seed correlation used these defined ROIs ($n = 29$ sessions, target; $n = 32$ sessions, distractor).

Seed Correlation Analysis

Correlation maps were trialwise generated for target and distractor hemispheres and for wS1, wMC, ALM, RSP, and limb S1 seed regions of interest (ten maps per session). Seed regions were defined as the mean of the pixels in the indicated ROI (rectangles defined above). Pairwise correlation coefficients were calculated between the defined seed region and all other pixels. The R^2 values are reported as the square of the pixelwise correlation coefficient.

Stimulus Encoding in Post-Stimulus Fluorescence

Stimulus encoding was quantified as the neurometric d' (Britten et al. 1992) of prestimulus fluorescence (stimulus absent) and post-stimulus fluorescence (stimulus present) during the lockout epoch, as previously applied to imaging data (Aruljothi et al. 2020). We excluded session data from this analysis if there

were fewer than four incorrect trials in the session (excluding five sessions for target Miss, two sessions for distractor FA). Neurometric d' was calculated separately according to target and distractor assignment and then according to trial type outcome. This resulted in six different datasets for stimulus encoding: all target trials, all distractor trials, hit trials, miss trials, false alarm trials, and correct rejection trials. Prestimulus and post-stimulus fluorescence histograms were plotted into receiver operating characteristic (ROC) curves and the area under the curve (AUC) was converted to d' as the neurometric:

$$\text{fluorescence } d'_{\text{Stimulus}} = \sqrt{2} * Z_{\text{AUC}}$$

Region specific pixel values for stimulus encoding were identified as the maximum value within the defined ROI, performed for target-aligned and distractor-aligned regions of wS1, wMC, and ALM. The difference in stimulus encoding in wS1 between the response and the no response trials for both target and distractor stimuli was calculated as the percentage:

$$\%_{\text{difference}} = \frac{\text{response trial} - \text{no response trial}}{(\text{response trial} + \text{no response trial}) / 2} * 100$$

Whisker Motion Energy during Behavior

The imaging window was cropped by region of interest: target or distractor paddle stimulus or whisker fields. The function "vision.VideoFileReader" was used for optimal reading of video frames into MATLAB. Whisker movement per frame (Δframe) was calculated as the pixelwise frame by frame mean gray value (MGV) difference ($\Delta\text{MGV}_{\text{pixel}}$). Whisker motion energy (WME) was defined as the sum of the squares across pixels:

$$\text{WME} = (\Delta l)^2 = \sum_{\text{pixels}} \left(\frac{\Delta\text{MGV}_{\text{pixel}}}{\Delta\text{frame}} \right)^2$$

WME traces of the cropped videos of the paddles were used to detect stimulus events (target/distractor). This was performed by using a constant threshold and aligning detected events from the video to their temporally closest events recorded using Arduino. The traces from the cropped videos of whisker fields were transformed (z-scored) to have a mean of zero and standard deviation of 1 for the purpose of comparison across sessions. Subsequently, WME data were temporally aligned by trial type to stimulus onset (target/distractor) determined from the videos. The prestimulus analysis window was the 500 ms preceding stimulus onset.

Principal Component Analysis of Fluorescence

All principal component (PC) analyses and statistics were performed in Python. Fluorescence was averaged across anatomic masks [target and distractor wS1, wMC, ALM, and retrosplenial (RSP) cortex] per frame per trial per session. Mean regions were normalized and placed into a covariance matrix. The covariance matrix was decomposed into an eigenmatrix, eigenvectors were sorted by eigenvalue weight, and eigenvectors were projected into component space. All frames were separated by trial type, plotted in PC space, and differentiated by trial epoch (prestimulus, post-stimulus and pre-response lockout, and allowable response window). Component data for prestimulus frames

were further analyzed: confidence area ellipses of 1 SD, σ, was defined by the ellipsoid distribution of prestimulus frames in PC space per session. Centroids were defined as the geometric mean of prestimulus frames in PC space per session.

Spike Sort and Cluster of Single Units

Using Neuronalynx recording system, signals were sampled at 32 kHz, band-pass filtered from 0.1 to 8000 Hz (wideband), and high-pass filtered at 600–6000 Hz (for spike detection). Putative spikes crossed thresholds of 20–40 μV, isolated from baseline noise. KlustaKwik algorithm in SpikeSort3D software was used for spike sorting and clustering. Clusters were defined by waveform and cluster location in feature space (peaks and valleys); movement artifacts (atypical waveforms or those occurring across all channels) were removed, as previously reported (Zareian et al. 2021). Subsequent analyses were conducted using MATLAB software (MathWorks). For analyses of population data, spike times of single units from each recording session were combined into a multiunit.

Sensory and Motor Encoding of Single Units

Sensory and motor encoding of single units was performed as previously reported (Zareian et al. 2021). Sensory encoding was quantified by the neurometric d' using stimulus absent spiking (300 ms prestimulus) and stimulus present spiking (100 ms post-stimulus). Motor encoding was quantified by the neurometric d' using response absent spiking (300 ms prestimulus) and response present spiking (100 ms pre-response). Distributions were plotted into ROC curves and the AUC was converted to d' as a neurometric:

$$\text{spike } d'_{\text{sensory}} \text{ or } d'_{\text{motor}} = \sqrt{2} * Z_{\text{AUC}}$$

Choice Probability of Single Unit and Multiunit Data

For choice probability analyses, we ensured that there was a minimum of five trials per trial type (minimum five Hits and five Miss). Choice probability (%) was quantified as the separation of prestimulus spiking in Hits versus Miss trials. ROC and AUC were calculated from the distributions of Hits and Miss across trials, 500–0 ms before stimulus onset, averaged over 50 ms nonoverlapping intervals, as previously reported (Zareian et al. 2021).

Local Field Potential Analyses

A single middle site from each silicon probe recording was used for local field potential (LFP) analyses; use of other sites led to qualitatively similar results (data not shown). To obtain the LFP, wideband signals were down-sampled to 200 Hz using MATLAB function "decimate". Power spectral densities were calculated using the welch method (MATLAB function "pwelch"). Frequency resolution step for calculating power was 0.78 Hz. Subsequently, trial-by-trial spectral densities were averaged from a 1-s period before stimulus onset and pooled across all trials and sessions. For spike triggered average (STA) analyses, we used the 400 ms window surrounding each prestimulus spike (±200 ms) for power analyses. We included spikes from 1 s to 200 ms before the stimulus so that STA windows would not overlap with the stimulus onset. For STA power calculation, LFP signals

and spikes were not analyzed from the same recording site to minimize spike waveform artifacts (Fries et al. 2001).

Statistical Analyses

For imaging statistics, threshold for statistical significance was corrected for multiple comparisons with a Bonferroni correction. For all dF/F and dF/F differences (Miss–Hits, CR–FA, means, SD), statistical analyses determined whether dF/F frames were significantly different than zero across sessions (one sample t-test). For region specific dF/F of Hits-Miss trials across defined ROIs, statistical analysis determined whether dF/F within ROIs was significantly different from zero (one-sample t-test) and whether dF/F across ROIs was significantly different from each other (one-way ANOVA and multiple comparison Tukey–Kramer test). For analyses of correlations between dF/F and RT within ROIs, statistical analyses of region-specific linear regression determined whether slopes within ROIs were significantly different from zero (one-sample t-test) and whether slopes across ROIs were significantly different from each other (one-way ANOVA).

For whisker analyses statistics, since the number of samples in the whisking data were low, we used one-sample Kolmogorov–Smirnov test ("kstest" in MATLAB) to test for normality assumptions. Since the data mostly violated the normality assumption, Wilcoxon signed rank ("signrank" in MATLAB) and rank sum ("ranksum" in MATLAB) tests were used for comparisons between prestimulus and post-stimulus whisking and between trial types (Hits vs. Miss, FA vs. CR), respectively. For stimulus encoding (neurometric d'), statistical analyses determined whether the trialwise (Hits, Miss, FA, CR) maximum pixel value in wS1 was significantly different than zero across sessions (one sample t-test). For differences in stimulus encoding, statistical analyses determined whether the stimulus-aligned wS1 maximum pixel value was significantly different between response (Hits, FA) and no response (Miss, CR) outcome types across sessions (two sample t-test). For PCA ellipsoid variance and centroid distribution, statistical analysis determined whether ellipsoid variance or centroid distribution was significantly different between response and no response prestimulus frames, evaluated per component. Box whisker plots show the distribution of prestimulus frames or ellipsoid centroids per trial type with outliers, evaluated per component.

For choice probability of single units, statistical analysis determined whether distributions within regions were significantly different from chance (one-sample t-test, chance level 50%) and whether distributions between regions were significantly different from each other (ANOVA and post-hoc Tukey test). For the significance assessment of sensory and motor encoding of single units, one-sample t-test was used to compare d-prime distributions to zero. For the relationship between sensory and motor encoding and choice probability of single units, statistical analysis determined whether regression slopes were significantly different from zero (95% confidence bounds for slopes). Box whisker plots were used to show distributions of sensory encoding, motor encoding, and choice probability of single units evaluated within regions. Single unit and multi-unit average data are presented as mean ± standard error of the mean, unless otherwise indicated. For LFP and STA LFP power comparisons between hit and miss or FA and CR trials, statistical analysis determined whether response trials were different from no response trials for each frequency step (paired t-test, $P < 0.01$).

Results

Global Prestimulus Activity Predicts Response Outcomes

We considered how prestimulus activity may influence sensory detection (Fig. 1A–D). High prestimulus activity may promote detection of target and distractor stimuli; alternatively, low prestimulus activity may promote detection of target and distractor stimuli or discrimination of target from distractor stimuli (Fig. 1A). The prestimulus activity that influences behavioral outcomes may present focally in specific task-related regions or globally across neocortex (Fig. 1B). A low variability, specific "optimal state" configuration may promote stimulus detection or target/distractor discrimination (Fig. 1C). At the level of single units, prestimulus contextual signals and post-stimulus sensory and motor signals may be carried by distinct neuronal ensembles (sparse coding) or overlapping neuronal ensembles (dense coding) (Fig. 1D). We tested these possibilities in a selective whisker detection task, in which head-fixed mice learn to respond to rapid deflections in one whisker field (target) and ignore identical deflections in the opposite whisker field (distractor) (Fig. 1E). In this task, the possible trial outcomes include hit (response to target), miss (no response to target), false alarm (FA, response to distractor), and correct rejection (CR, no response to distractor) (Fig. 1F). Prior to each stimulus was a variable inter-trial interval (ITI), in which mice were required to withhold responding or else reset the ITI. The prestimulus epoch we used for analyses is the last 1 s of the ITI immediately prior to stimulus onset (Fig. 1G).

We used widefield Ca²⁺ imaging to measure neuronal activity during expert task performance in frontal and parietal cortices, bilaterally (Fig. 1E). Our imaging dataset consists of 38 imaging sessions from 5 mice, using a single task-engaged period per session (see Methods). Due to the highly lateralized cortical whisker representation, we could clearly define target-aligned and distractor-aligned cortical regions, contralateral to the side of the whisker stimulus. To preserve activity fluctuations prestimulus, we normalized raw fluorescence activity using a sliding window method (400 s sliding window, see Methods and Supplementary Fig. 1).

In Figure 2 we present grand average fluorescence activity for each trial outcome, aligned to the onsets of both the stimulus and response. In the first column of Figure 2 we show the last prestimulus frame, which is representative of the full prestimulus epoch (Supplementary Fig. 2A). We note stark differences in prestimulus activity for different trial outcomes, particularly when comparing hit (Fig. 2A) and miss (Fig. 2D) trials. We observed lower prestimulus activity for hit versus miss and for FA versus CR trials, indicating that lower prestimulus activity precedes "response" compared to "no response" outcomes. Interestingly, low prestimulus activity appears to be specifically related to stimulus detection rather than response preparation. This is evidenced by higher activity preceding spontaneous responses (Spont, a response during the ITI, Fig. 2C) compared to stimulus-related responses (hits and FA, Fig. 2A,B). The magnitude of the prestimulus differences is large, on the same scale as the post-stimulus activity. Additionally, prestimulus activity suppression preceding response trials appears to be widely distributed throughout dorsal neocortex, rather than being focused on the task-related regions of wS1, wMC and ALM.

We quantified the differences in prestimulus activity between response and no response trials for target and distractor stimuli (Fig. 3A–F). Shown in this figure are data from the last

500 ms of the prestimulus (similar results were obtained using 1 s prestimulus epochs, Supplementary Fig. 2C,E). We subtracted the average prestimulus fluorescence activity of hit from miss trials (Fig. 3A). The positive values indicate higher activity preceding miss compared to hit trials ($n = 29$ sessions, averaged across the entire field of view: dF/F $\mu_{[Miss\text{-}Hits]} = 2.1\% \pm 0.3\%$; one-sample t-test, $t(28) = 8.1$, $P = 7.9e{-}09$). The largest differences were not in the task-related whisker (wS1, wMC) or licking (ALM) regions but appear to be focused on the limb regions of somatosensory cortex. While dF/F is already a normalized metric, we sought to further control for possible regional differences in imaging sensitivity. Therefore, we conducted the same subtraction analysis, but on normalized dF/F values, indexed using the pixelwise mean and SD across sessions. With this analysis (Fig. 3B), the activity differences are more uniformly distributed across frontal and parietal cortices, with an average miss-hit difference of 1.2 SD.

To determine the spatial regions of significance, on each pixel we performed a one-sample t-test on average prestimulus activity in miss minus hit fluorescence maps across sessions (P-value of each pixel shown in Fig. 3C). All neocortical regions within our field of view demonstrated statistical significance, even with a Bonferroni corrected alpha level to control for multiple comparisons (28 960 pixels). Thus, lower prestimulus activity on upcoming target trials is predictive of hit versus miss outcomes. This is observed for all cortical regions within our field of view, including task-related and task-unrelated regions. Similar findings were obtained for measures of variability (Supplementary Fig. 2B,D,F), with increased SD of prestimulus activity on miss compared to hit trials globally throughout dorsal cortex.

There were some notable similarities and differences for distractor trials (Fig. 3D–F). Similar to target trials, higher activity was observed preceding no response (CR) versus response (FA) trials ($n = 32$ sessions, averaged across the entire field of view: dF/F $\mu_{[CR\text{-}FA]} = 0.36 \pm 0.11\%$ one-sample t-test, $t(31) = 3.38$, $P = 0.002$). However, the fluorescence differences were approximately 5-fold higher for target trials compared with distractor trials (dF/F $\mu_{[Miss\text{-}Hits]} = 2.1\%$ vs. $\mu_{[CR\text{-}FA]} = 0.36\%$). A second difference is that for distractor trials, the focus on the somatosensory limb regions was observed in dF/F, SD, indexed, and P-value maps (Fig. 3D–F, Supplementary Fig. 2B,D,F). The regions with the lowest P-value were slightly above the Bonferroni corrected alpha level. Thus, while lower activity preceding distractor trials was also predictive of a response, the effect size was smaller and less widespread.

In addition to predicting response outcome, we also sought to determine whether prestimulus activity levels predict reaction time on response trials (Fig. 3G–J). For these analyses, we determined the slope and coefficient of determination (R^2) of linear fits for prestimulus dF/F versus reaction time for Hit and FA trials (separately) for each session. As shown in the example session in Figure 3G, a positive slope indicates a correlation between higher prestimulus activity and longer post-stimulus reaction times. Across all sessions, we found a significant positive correlation (positive slope) on Hit trials between prestimulus activity and reaction time ($n = 30$ sessions, slope $= 0.64 \pm 0.23$, one-sample t-test: $t(29) = 2.73$, $P = 0.011$; $R^2 = 0.074 \pm 0.023$) (Fig. 3H). Thus, for target stimuli, lower prestimulus activity predicts both Hit versus Miss outcomes and faster reaction times. We performed the same regression analyses for FA trials (Fig. 3J). In contrast to Hit trials, FA trials across sessions did not show consistent correlations between prestimulus activity and
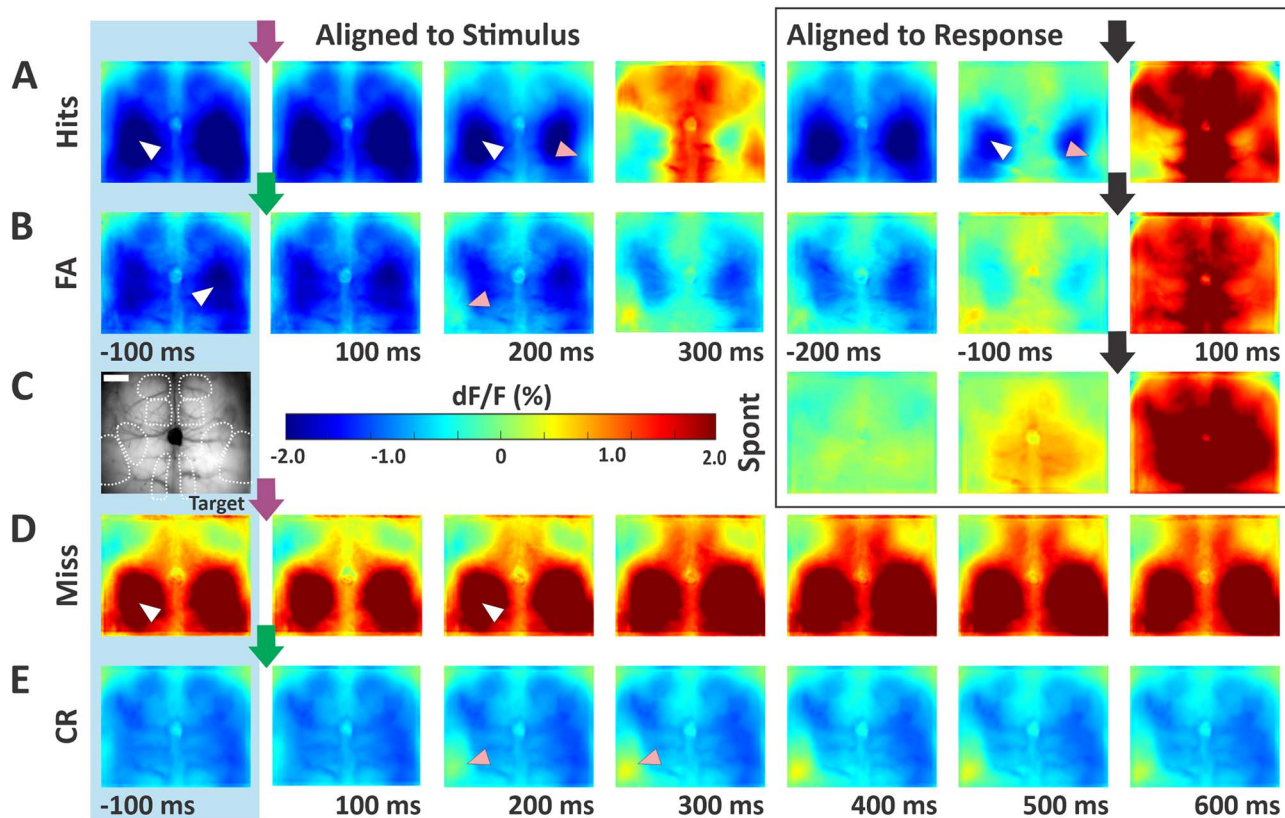
Figure 2. Sliding window normalized grand average fluorescence activity (dF/F). Data are averages across all mice and all sessions ($n = 38$ sessions). Activity in specific imaging frames is aligned to the stimulus onset (left, purple and green arrows for target and distractor stimuli, respectively) or response onset (black frame, black arrows, in rows A, B, and C). Warmer colors indicate higher activity (scale bar in row C applies to all panels). The pink arrowheads specify stimulus-aligned whisker regions of S1, whereas the white arrowheads specify limb regions of S1 (see atlas in leftmost panel in row C). The last prestimulus frame is shown in the first column (blue shade). Shown are hit trials (A), false alarm trials (B), spontaneous trials (C), miss trials (D), and correct rejection trials (E). Note the low (negative due to normalization) dF/F prestimulus activity in response trials (hit and false alarm), compared to the high dF/F prestimulus activity in miss trials. Scale bar in (C) is 1 mm.

reaction time ($n = 32$ sessions, slope $= -0.45 \pm 1.48$, one-sample t-test: $t(31) = -0.3$, $P = 0.76$; $R^2 = 0.12 \pm 0.021$) (Fig. 3J).

The above analyses demonstrated that lower prestimulus activity broadly across dorsal cortex predicted response (vs. no response) outcomes and faster reaction times (for hit trials). Subsequent analyses determined if these correlations displayed regional differences. We defined regions of interest (ROIs) bilaterally (target-aligned and distractor-aligned: wS1, wMC, ALM, retrosplenial cortex (RSP), limb S1). For Hits-Miss prestimulus dF/F, parietal regions (wS1, RSP, and limb S1) showed significantly larger differences compared to frontal regions (wMC and ALM) (one-way ANOVA, $F(289) = 7.53$, $P = 7.1\text{e}{-}10$, post-hoc multiple comparisons) (Supplementary Fig. 3). However, we did not observe differences among these ROIs in the relationships between prestimulus activity and reaction time (Supplementary Fig. 4) (one-way ANOVA, Hits: $F(149) = 0.63$, $P = 0.64$, FA: $F(159) = 0.2$, $P = 0.94$).

In addition to analyzing these regions individually, we also determined whether their prestimulus spatial correlations predicted response outcomes. We defined seed ROIs as above, and determined the pairwise correlations across prestimulus frames for each pixel (Supplementary Fig. 5). Interestingly, this analysis revealed widespread spatial correlations preceding no response trials (higher R^2 values outside of the seed region). Inversely, our data demonstrate spatial "decorrelation" preceding response

trials. Similar patterns were observed for both target and distractor trials (Supplementary Fig. 5A,B, respectively).

Contributions of Stimulus Encoding and Movement on Trial Outcomes

Next, we assessed whether the differences in trial outcome were reflected in differences in stimulus responses in the neocortex. We quantified the stimulus encoding during the lockout period (200 ms post-stimulus and pre-response) for each trial type (Fig. 4). For each pixel, we measured stimulus encoding as the neurometric sensitivity index d' (Fig. 4A–F) and determined whether these values were significantly different from zero (Fig. 4G–L). We observed significant stimulus encoding in the stimulus-aligned primary somatosensory cortex (wS1) for each trial type (one-sample t-test, $n = 38$, hits: 38, miss: 33, FA: 36, CR: 38, hits: d' $\mu_{wS1} = 0.98 \pm 0.06$, $t(37) = 15.58$, $P = 7.79\text{e}{-}18$; miss: d' $\mu_{wS1} = 0.69 \pm 0.08$, $t(32) = 9.08$, $P = 2.26\text{e}{-}10$; FA: d' $\mu_{wS1} = 1.05 \pm 0.09$, $t(35) = 12.08$, $P = 4.87\text{e}{-}14$; CR: d' $\mu_{wS1} = 0.58 \pm 0.049$, $t(37) = 11.89$, $P = 3.32\text{e}{-}14$). Thus, significant stimulus responses occur in wS1 for both response and no response trials. However, we did observe a 40–60% reduction in wS1 stimulus encoding in no response compared to response trials for target and distractor stimuli (hits vs. miss: d' $\mu_{\%\text{ difference}} = 39.84 \pm 7.44\%$, paired-sample t-test,
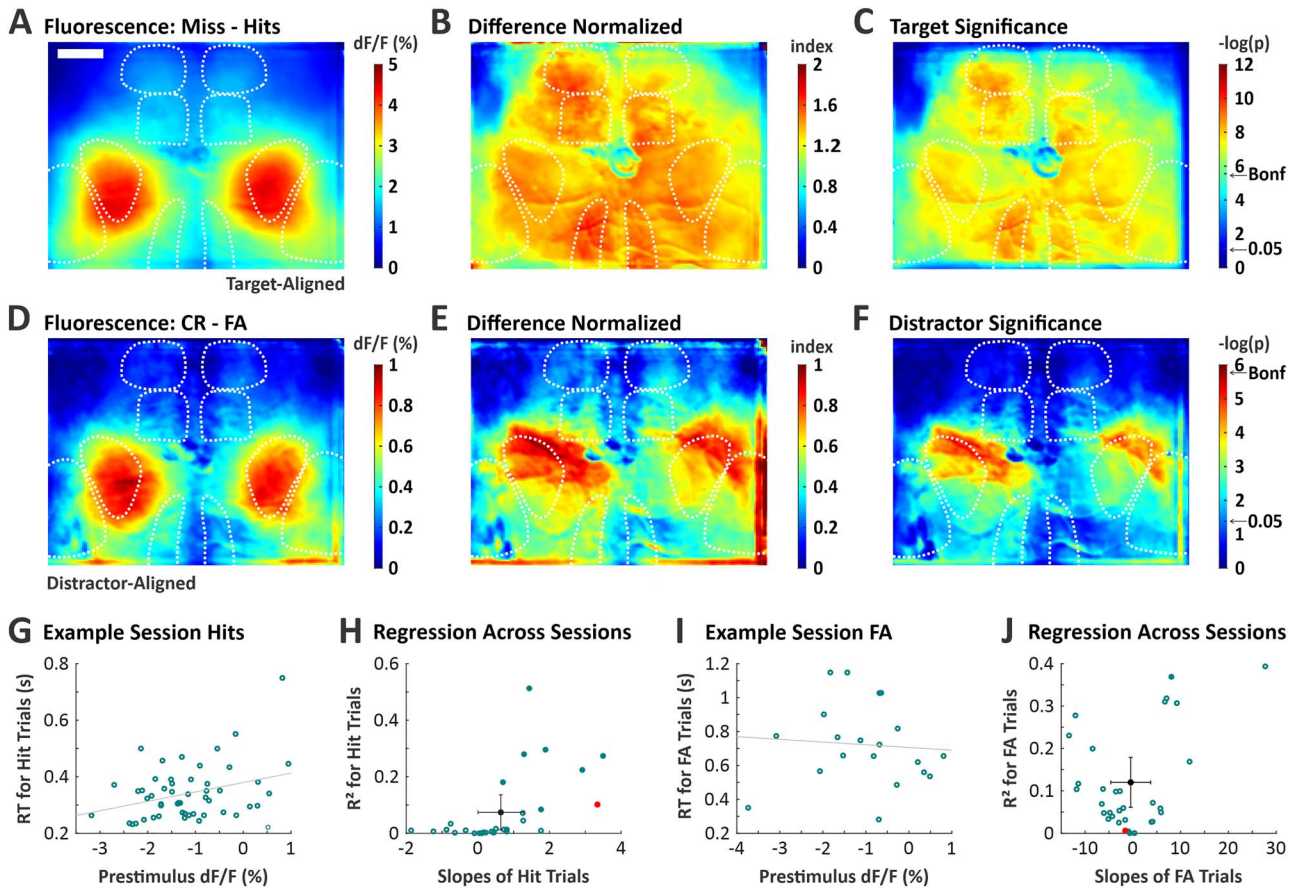
Figure 3. Prestimulus neuronal activity differences between response and no response trials and correlations with reaction time. (A) Grand average of prestimulus dF/F for miss minus hit trials. All pixel values within neocortex are greater than 0, indicating higher global activity preceding miss trials. (B) Similar to (A), except that the individual session dF/F signals were further indexed (μ/σ) to normalize for differences in fluorescence fluctuations. (C) Significance map for the data in (A). Significance threshold with Bonferroni correction for multiple comparisons is indicated by the arrow (Bonf). For target trials, higher activity preceding no response trials is statistically significant throughout dorsal cortex. (D–F) Same structure as (A–C), except for CR minus FA trials. Note the more restricted range of scale bars in each panel, compared to target data. For distractor trials, higher activity preceding no response trials is marginally significant, most prominent in the limb S1 regions. Scale bar in (A) is 1 mm. (G) An example session showing a positive correlation between prestimulus activity (dF/F) and reaction time for individual Hit trials (slope $= 3.34$, $R^2 = 0.10$, dotted line is the linear regression). (H) Regression analyses across all sessions for Hit trials. The red data point is the example session in (G), the black data reflect the mean $\pm$ SD across sessions ($n = 30$ sessions). (I) FA trials in an example session, with a non-significant negative correlation between prestimulus activity and reaction time (slope $= -1.6$, $R^2 = 0.006$). (J) Same as H but for FA trials ($n = 32$ sessions).

$t(32) = 4.51$, $P = 8.26\text{e}{-}05$; FA vs. CR: d' $\mu_{\%\text{ difference}} = 61.62 \pm 7.26\%$, paired-sample t-test, $t(35) = 6.72$, $P = 8.75\text{e}{-}08$, see Methods). In summary, response trials are associated with reduced prestimulus activity and enhanced post-stimulus sensory responses.

Recent studies have demonstrated widespread neuronal activity increases due to movement (Stringer et al. 2019; Musall et al. 2020; Salkoff et al. 2020). Therefore, in a separate set of recordings, we determined the magnitude of prestimulus and post-stimulus whisker movements on different trial outcomes. Whisker movement was quantified as whisker motion energy (WME, normalized by z-score, see Methods). In Figure 5A–C we present these analyses for one example session for target stimuli. On hit trials, WME increased dramatically post-stimulus (Fig. 5A, purple trace). We interpret this as whisking being part of the "uninstructed" behavioral response sequence (Musall et al. 2020). Importantly, we also observed differences in WME prestimulus, with higher WME on miss compared to hit trials (mean $\pm$ STD WME $\mu_{\text{Hits}} = -0.45 \pm 0.32$, WME $\mu_{\text{Miss}} = 0.19 \pm 0.71$, rank sum $= 1516$, $P = 0.001$, two-sided Wilcoxon rank sum

test; Fig. 5A,B). In Figure 5C, we show prestimulus WME for each target trial, with the color of the bar indicating trial outcome. High prestimulus WME was more likely to result in a miss trial, even though many miss trials were not preceded by high prestimulus WME. Similar results were observed across all sessions ($n = 9$ session, Fig. 5D, Wilcoxon sign rank test, mean $\pm$ STD prestimulus WME $\mu_{\text{Hits}} = -0.12 \pm 0.17$ vs. prestimulus WME $\mu_{\text{Miss}} = 0.12 \pm 0.15$, signed rank $= 1$, $P = 0.008$). Thus, high prestimulus movement was associated with some, but not all, of the miss trials.

Differences in prestimulus WME were not as pronounced on distractor trials (Fig. 5E–H). We did notice a trend towards increased WME on CR trials. However, this effect was not statistically significant across sessions ($n = 9$ session, Fig. 5H, Wilcoxon sign rank test: prestimulus WME $\mu_{\text{FA}} = -0.14 \pm 0.2$ vs. prestimulus WME $\mu_{\text{CR}} = -0.04 \pm 0.10$, signed rank $= 8$, $P = 0.098$). Notably, the effects of prestimulus movement on target and distractor trial outcomes parallel the effects of prestimulus neuronal activity: low prestimulus neuronal activity and low prestimulus WME predict response outcomes, yet these effects are
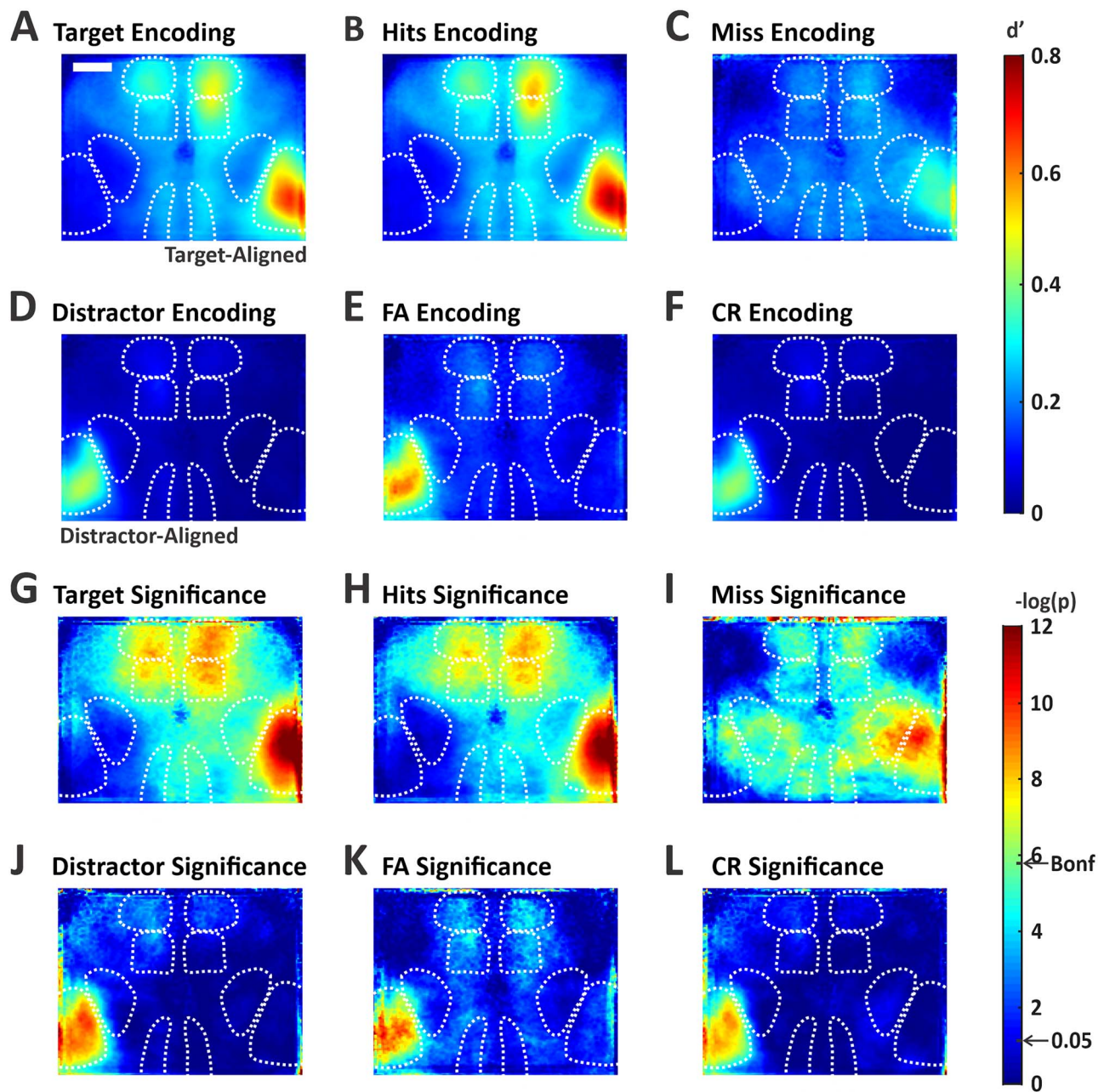
Figure 4. Quantification of stimulus encoding for each trial type. (A–F) Neurometric d' values were calculated for each pixel during the last frame of the lockout: after stimulus presentation and before the allowed response window. Data are grand average d' maps from all sessions, showing all target trials (A), hit trials (B), miss trials (C), all distractor trials (D), FA trials (E), and CR trials (F). Note the larger stimulus encoding in response trials (B and E compared to C and F). Significance maps of the data in (A–F), respectively. Significance threshold with Bonferroni correction for multiple comparisons is indicated by the arrow (Bonf). For all trial types there is significant stimulus encoding in the stimulus-aligned S1 whisker region. Scale bar in (A) is 1 mm.

much more pronounced for target compared to distractor trials.

Analyses of Prestimulus Activity Variance and Subspace in Reduced Spatial Dimensions

Next, we sought to characterize frame-by-frame variability in our imaging data. To accomplish this, we used principal component analysis (PCA) to reduce the spatial dimensionality (Fig. 6). First, we extracted regional single-trial fluorescence activity using anatomic masks from the dorsal neocortex centered on regions of interest: target/distractor wS1, RSP, wMC, and ALM (Fig. 6A). We concatenated data from all frames, trials, sessions, and mice and performed PCA on this combined matrix. This enabled us to convert all sessions into the same lower-dimensional axes. Most of the variability in our imaging data could be explained by the first component (~91%) and the first two components explained ~96% of the variance (Fig. 6B–D). Therefore, further analyses focused on these first two spatial components.
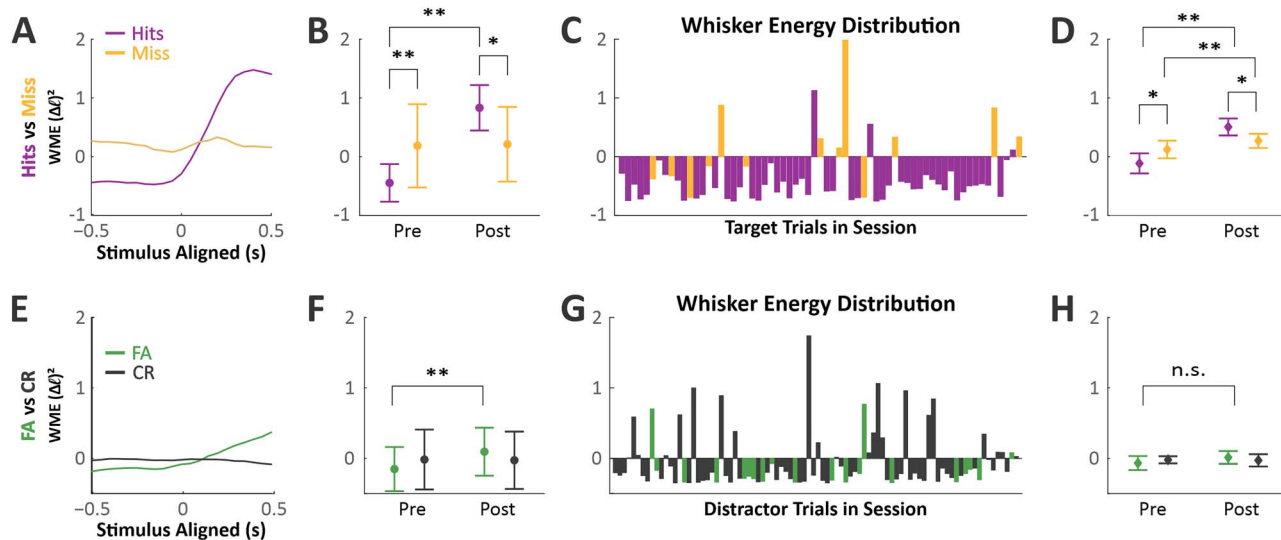
Figure 5. Prestimulus and post-stimulus whisker movements in each trial type. (A) Peristimulus whisker motion energy (WME) on target trials in an example session, hits (purple) and miss (orange). On hits trials there was a dramatic increase in WME post-stimulus and during the response window. Prestimulus, however, WME on hits trials was reduced compared to miss trials. (B) Quantification of data in (A), comparing prestimulus (pre) and post-stimulus (post) WME for hit and miss trials. (C) Prestimulus WME values for each trial in the example session. (D) Summary data for all sessions ($n = 9$). Note the reduced WME preceding hit compared to miss trials. (E–H) Same as above, but for distractor trials. While this example session shows moderately reduced WME preceding false alarm trials (E–G), this trend was not statistically significant across the full dataset (H). Data are presented as mean ± SD, *$P < 0.05$, **$P < 0.005$.

We determined the distributions of prestimulus activity from single frames within this PCA space (Fig. 7). In Figure 7A, we plot the data from two example sessions, in which each data point is a single prestimulus frame preceding a hit (purple) or miss (yellow) trials. We noticed that the data from hit trials were more tightly clustered than the data from miss trials. To quantify this observation, first we fit the data from each trial type with a covariance ellipse. The shaded ellipses in Figure 7A represent a confidence area of 1 SD, σ, which we used as a measure of framewise variability. Figure 7B plots the confidence area for prestimulus activity on hit and miss trials for all sessions ($n = 29$ sessions). The prestimulus activity variance is significantly lower for hit compared to miss trials (effect size, Cohen's $d = 1.92$; paired t-test, $t(28) = 9.43$, $P = 1.74e{-}10$).

We conducted the same analyses for distractor trials and obtained similar results. The two example sessions in Figure 7C show more tightly clustered prestimulus activity for response (FA) compared to no response (CR) trials. Across all sessions ($n = 32$), the confidence areas are significantly lower for FA compared to CR trials (effect size, Cohen's $d = 1.11$; paired t-test, $t(31) = 7.40$, $P = 1.22e{-}8$, Fig. 7D). Thus, for both target and distractor trials, lower framewise prestimulus variability predicts response outcomes.

In addition to differences in variability, we also noticed that the prestimulus activity resides in different subspaces preceding response and no response trials. As evident in Figure 7A, "within" each session the centroids of the hit and miss confidence areas are offset, whereas "between" these two sessions the hit centroids occur at similar positions. In Figure 7E, we plot the centroid position for all sessions ($n = 29$ sessions). Indeed, we find that across all sessions the centroid positions preceding hit trials are separated from the centroid positions preceding miss trials. For target trials, this separation is significant, for both PC1 and PC2 axes (Fig. 7F, PC1: $d = 2.19$, paired t-test, $t(28) = 8.55$, $P = 1.34e{-}9$; PC2: $d = 1.24$, $t(28) = 4.01$, $P = 2.07e{-}4$). In contrast, for distractor trials, the centroids of prestimulus activity show

greater overlap for response (FA) and no response (CR) trials (Fig. 7G). However, we do still find significantly different centroid positions on distractor trials along PC1 (Fig. 7H, PC1: $d = 0.57$, paired t-test, $t(31) = 2.99$, $P = 0.0027$; PC2: $d = 0.43$, $t(31) = 1.30$, $P = 0.10$). These data indicate that the neuronal activity across dorsal neocortex preceding response trials is less variable than no response trials and occupies a separate subspace. Additionally, like prestimulus neural activity (Fig. 3) and movement (Fig. 5), the differences in variability and subspace position are larger for target compared to distractor trials. Taken together, these data specify an optimal neuronal and behavioral state for stimulus detection.

Distribution of Prestimulus Choice Probability among Single Units

The above analyses of widefield imaging data assessed population neuronal activity. In this series of analyses, we sought to determine the distribution of task-relevant prestimulus activities among single units (Fig. 8). During the same selective whisker detection task, we recorded 936 single units, from target-aligned wS1 (377 units), target-aligned wMC (338 units) and target-aligned ALM (221 units). First, we quantified the prestimulus choice probability of all units on target trials. Choice probabilities (CP in %) of single units in each region were marginally below chance (50%) (Fig. 8A, CP $\mu_{wS1} = 49.10 \pm 0.16$, one-sample t-test, $t(376) = -5.72$, $P = 2.21e{-}8$, CP $\mu_{wMC} = 49.44 \pm 0.2$, one-sample t-test, $t(337) = -2.82$, $P = 0.005$, CP $\mu_{ALM} = 49.64 \pm 0.19$, one-sample t-test, $t(220) = -1.92$, $P = 0.06$). These distributions were not significantly different across the three regions (two-way ANOVA: $F(2,933) = 2.18$, $P = 0.11$ and post hoc Tukey: wS1 vs. wMC, $P = 0.33$; wMC vs. ALM, $P = 0.76$; wS1 vs. ALM, $P = 0.12$). To increase spike density, we combined single units from each session (Zareian et al. 2020) and calculated the average prestimulus choice probability for these multiunit ensembles across all sessions. This analysis generated a slightly
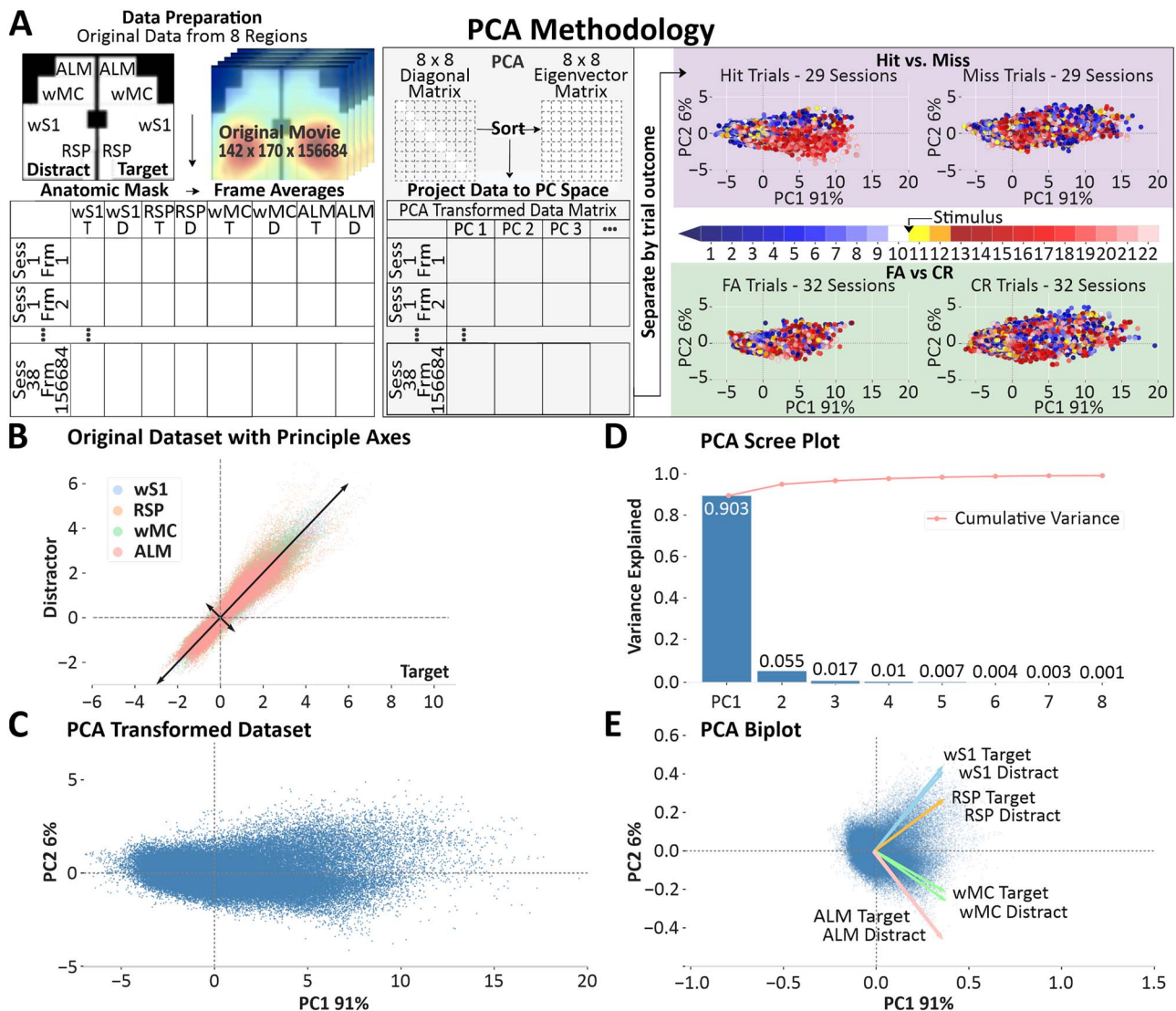
Figure 6. Spatial dimensionality reduction for single trial analyses. (A) Methodology for using principal component analysis (PCA) to reduce spatial dimensionality. Left, full images were parsed into eight regional masks. Average dF/F within each mask for all trials and all sessions were appended into a single matrix, upon which PCA was performed. Right, frames with different trial outcomes were back-projected to the first principal component (PC1) and plotted against their projection onto the second principal component (PC2). Transformed samples are colored based on their frame index: prestimulus (blue to white), post-stimulus and pre-response (yellow and orange), response (red to pink). (B) Original dataset, each data point represents a sample frame ROI-specific average, plotted against its change in fluorescence (dF/F) between target (x-axis) and distractor (y-axis) hemispheres. Black arrows represent the first two principal vectors. (C) Transformed dataset, each data point represents a sample frame plotted against its projection onto PC1 and PC2. (D) PCA scree plot. PCs are plotted according to their rank in variance, with accumulated variance plotted in red. The first two PCs were chosen for further analysis as they explain >95% variance of the untransformed dataset (PC1, 91%, PC2, 6%). (E) PCA biplot. Samples plotted against their normalized projection onto PC1 and PC2, with vectors representing individual ROIs according to their loadings.

lower prestimulus choice probability than the analysis of single units (all regions: $n = 43$ sessions, 47.62 ± 5.78, one-sample t-test, $P = 0.01$). Prestimulus choice probability below chance indicates that lower activity predicts hit compared to miss outcomes, and therefore is consistent with the widefield imaging data. However, the distributions of these data indicate that only a small portion of single units show strong prestimulus choice probability.

Given this variability of single units, we next asked whether the units with strong prestimulus choice probability overlap with the units with strong post-stimulus sensory and pre-response motor encoding. To test this, we plotted prestimulus choice probability against post-stimulus sensory

(Fig. 8A) and pre-response motor (Fig. 8B) encoding. The negative regression slopes show correlations between choice probability and sensory encoding for wS1, and between choice probability and motor encoding for wS1, wMC, and ALM (Fig. 8C,D, one-sample t-test, sensory encoding slope: $m_{wS1} = -1.96 \pm 0.31$, $t(375) = -6.34$, $P = 6.56e-10$; one-sample t-test, motor encoding slope: $m_{wS1} = -2.05 \pm 0.28$, $t(375) = -7.35$, $P = 1.23e-12$, $m_{wMC} = -0.64 \pm 0.26$, $t(336) = -2.49$, $P = 0.013$, $m_{ALM} = -0.96 \pm 0.28$, $t(219) = -3.46$, $P = 6.41e-4$). Thus, units in these regions have combined neuronal representations such that those representing prestimulus behavioral context overlap with those with post-stimulus (sensory) and pre-response (motor) task-relevant encoding. This overlap may be influenced
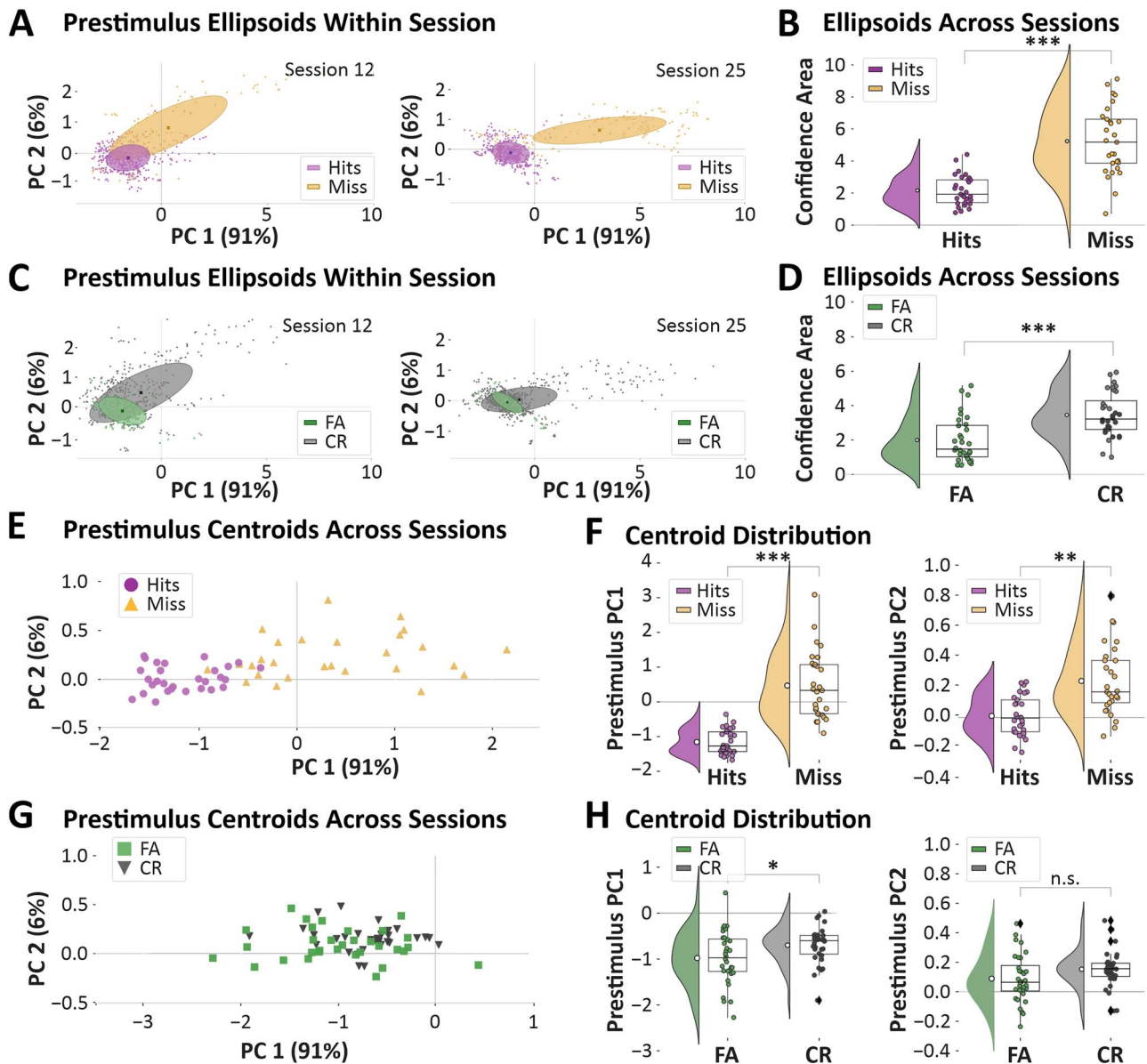
Figure 7. Single trial analyses of prestimulus subspace variance and position according to trial outcomes. All data presented are from the last 500 ms of the prestimulus window (frames 6–10 of Fig. 6A). (A) Prestimulus activity in PC space for hit (purple) and miss (yellow) trials of two example sessions. Each data point represents a single prestimulus frame. Overlaid are covariance ellipses for both trial outcome types (major radius, 1σ along PC1; minor radius, 1σ along PC2). Note the reduced area and distinct position of the covariance ellipses for hit compared to miss trials. (B) Comparison of the ellipse area, as a measure of variability, across all sessions. (C and D) Same as (A) and (B), except for FA (green) and CR (gray) trials. Response trials (hit and FA) are preceded by less variable prestimulus activity compared to no response trials (miss and CR). (E) Centroid positions of the covariance ellipses in PC space for all sessions, for hit and miss trials (same color designation as above). Each data point represents the hit or miss centroid from one session. (F) Quantification of centroid positions on axes PC1 (left) and PC2 (right). (G and H) Same as (E) and (F), except for FA and CR trials. Prestimulus activity occupies distinct subspaces for response and no response trials, along both PC1 and PC2 for target trials and along PC 1 for distractor trials. *$P < 0.01$; **$P < 0.001$; ***$P < 0.0001$; n.s., non-significant.

by a common factor such as firing rate (Supplementary Fig. 6). Nevertheless, these analyses demonstrate that the subset of neurons that show the largest prestimulus suppression on hit trials are the same neurons that strongly encode post-stimulus task features.

Prestimulus LFP Power and Spike-LFP Synchrony Do Not Predict Trial Outcome

Finally, we wondered whether the low amplitude, low variability prestimulus widefield Ca^{2+} signals preceding response trials

reflect changes in neuronal synchrony. Specifically, this activity profile may reflect low frequency desynchronization observed during behavioral states of high arousal (Harris and Thiele 2011; Zagha and McCormick 2014). To test this, we analyzed local field potentials (LFPs) recorded from layer 5 of the target-aligned wS1, wMC, and ALM (Fig. 9). First, we compared prestimulus LFP power preceding hit and miss trials. We did not observe difference in LFP power (0–50 Hz) across all regions combined and did not observe any differences in low frequencies (0–20 Hz) in each region analyzed separately (Fig. 9A–D). Similar results
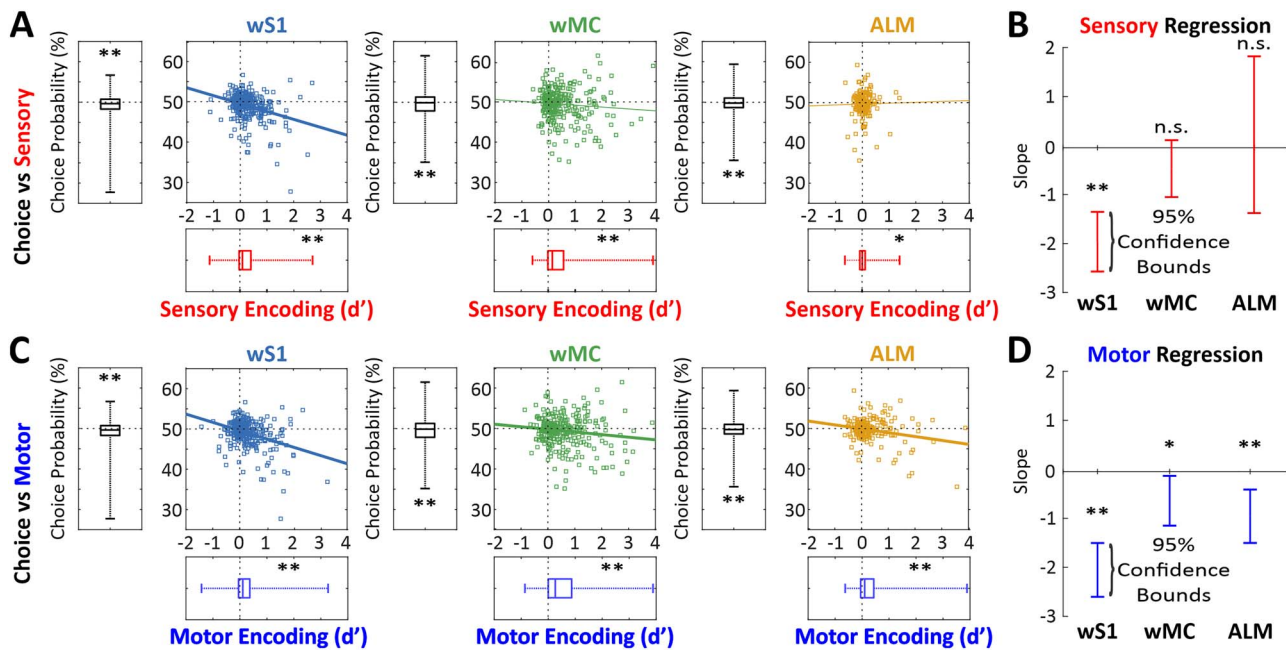
Figure 8. Distribution of prestimulus choice probability, post-stimulus sensory, and pre-response motor encoding across single units in wS1, wMC and ALM. (*A*) Plots of sensory encoding (*d'*) versus choice probability (%) for single units in target-aligned wS1 (left), wMC (center), and ALM (right). Asterisks above box plots reflect comparisons of individual measures to chance (*d'* = 0 and choice probability = 50%). Scatter plots include linear fits of the single unit data. Single units in each of these three cortical regions show below chance prestimulus choice probability (tending yet not significant for ALM (*P* = 0.06), significant for wS1 and wMC) and positive post-stimulus sensory encoding. (*B*) 95% confidence bounds of the linear regression slope values. (*C* and *D*) Same as (*A*) and (*B*), but for pre-response motor encoding. The significant negative slope values indicate an overlap between the single units with lower than chance prestimulus choice probability and positive post-stimulus sensory encoding (for wS1) and pre-response motor encoding (for wS1, wMC, and ALM). **P < 0.05; **P < 0.005; n.s., non-significant.*

were obtained for FA and CR trials (Supplementary Fig. 7A–D). Second, we measured the prestimulus spike-triggered average (STA) LFP, as a measure of spike-LFP synchrony. Similarly, we did not observe differences in prestimulus STA LFP preceding hit and miss trials (Fig. 9E–H) or FA and CR trials (Supplementary Fig. 7E–H). These negative findings suggest that the global activity differences observed in widefield Ca²⁺ imaging data are not due to a difference in neuronal synchrony.

Discussion

The primary focus of this study is to determine whether and how neuronal activity before stimulus onset predicts trial outcomes during goal-directed behavior. We assessed this for both target and distractor stimulus detection. We find that lower prestimulus activity predicts detection of both target and distractor stimuli (Figs 2 and 3) and faster reaction times on Hit trials (Fig. 3). This low activity state is distributed globally throughout dorsal cortex (Fig. 3), maps onto a distinct, less variable subspace than activity preceding no response trials (Fig. 7) and is represented most robustly in the subset of neurons also encoding post-stimulus sensory and pre-response motor task features (Fig. 8). Additionally, this global low-amplitude cortical state preceding response trials is associated with long-range spatial decorrelation (Supplementary Fig. 5) without changes in local synchronization (Fig. 9).

The impacts of spontaneous activity on stimulus responses have been explored extensively in both physiological and computational studies. Increased spontaneous activity has been proposed to increase response gain by two primary mechanisms: depolarization to reduce membrane potential

distance to spike threshold and increased variance to amplify the impacts of weak inputs (Hô and Destexhe 2000; Rudolph and Destexhe 2003; Shu et al. 2003; Haider et al. 2007; Cardin et al. 2008; Haider and McCormick 2009). Therefore, we were surprised to find that reduced prestimulus activity correlated with both enhanced stimulus detection (Figs 2 and 3) and increased sensory responses (Fig. 4). And yet, our data are consistent with studies in primary somatosensory and auditory cortices, demonstrating increased sensory responses with reduced prestimulus activity (Sachdev et al. 2004; Hasenstaub et al. 2007; Cardin et al. 2008; McGinley, David, et al. 2015a). Future studies are required to determine the cellular and network mechanisms underlying increased responsiveness with low activity, with possibilities including reduced membrane conductance (Chance et al. 2002), reduced inhibition, and reduced synaptic depression.

Our study was conducted in the context of a somatosensory (whisker) detection task in mice. It is not currently known, however, whether these findings will generalize to other sensory modalities and other types of tasks. Reduced network activity and reduced synaptic variance have been shown to predict a network with a discrete, all-or-none input–output function (Hô and Destexhe 2000). This configuration may improve distinguishing the presence versus absence of a stimulus as needed for stimulus detection. Such a network state, though, would be predicted to poorly encode the precise features of a stimulus. Therefore, we speculate that tasks requiring discrimination of fine stimulus details may be optimal in a high activity network state with a continuous input–output function. However, this remains to be tested.

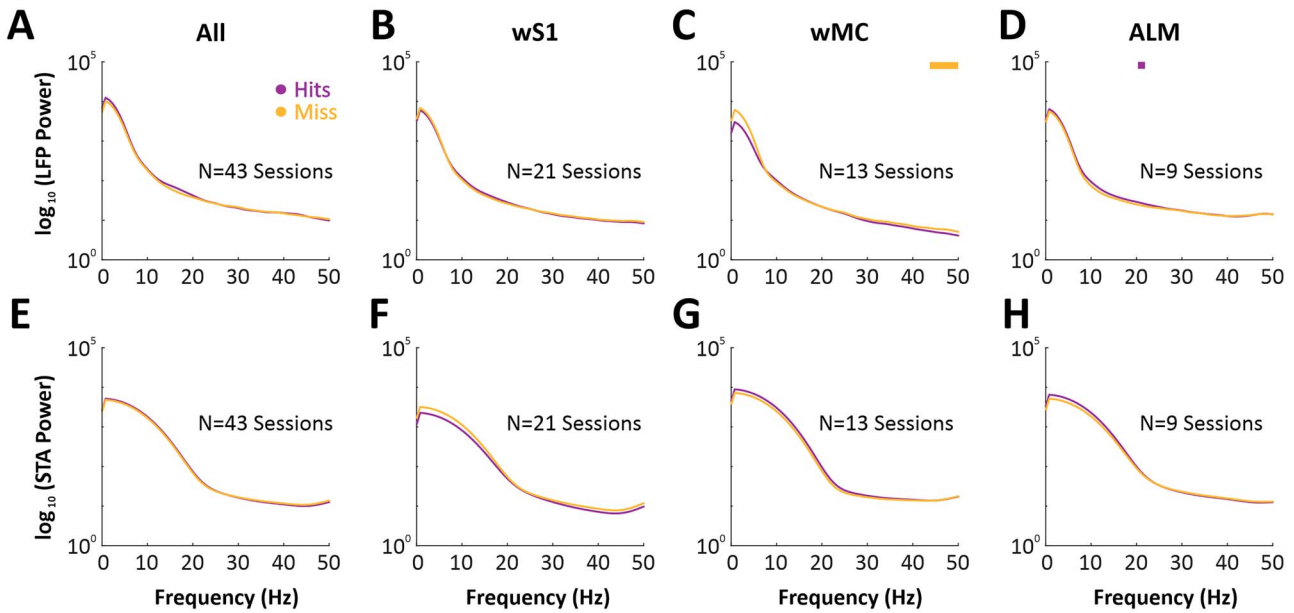Most studies of the impacts of spontaneous activity on sensory responses focus on primary sensory areas. However,

Figure 9. Lack of differences in LFP power and spike-triggered average LFP power preceding hit compared to miss trials. (*A–D*) Power spectra for local field potentials (LFPs) recorded from layer five across target-aligned regions combined (*A*) and separately calculated for (*B*) wS1, (*C*) wMC, and (*D*) ALM. Bars above plots reflect significance using paired *t*-test (P < 0.01) for each frequency step. Color of bar indicates direction of difference between LFP traces (purple for hits larger than miss, yellow for miss larger than hits). (*E–H*) Same as in (*A–D*), except for power spectra calculated from spike-triggered average (STA) LFPs.

stimulus detection tasks require the contributions of multiple cortices (De Lafuente and Romo 2006). Indeed, we have recently shown that the task in this study activates multiple sensory and motor cortices, including wS1, wMC, and ALM (Aruljothi et al. 2020; Zareian et al. 2021). In this study we demonstrate that the prestimulus activity predictive of trial outcome is global, involving all regions of dorsal neocortex. This global cortical state may reflect the coordination among multiple cortices, to improve not just stimulus encoding in primary sensory cortex, but the propagation of task-relevant signals throughout neocortex. Interestingly, we found prestimulus activity suppression to be largest in the same neurons that also strongly encode post-stimulus sensory and pre-response motor features, in wS1, wMC, and ALM. This organization may ensure coordination not just between cortical regions, but among the specific neuronal ensembles involved in this stimulus detection task. Low activity in these specific neuronal ensembles may increase excitability and transmission by increasing membrane resistance and reducing synaptic depression.

Global changes in cortical state, as observed here, are traditionally associated with changes in arousal, driven by widespread ascending neuromodulatory systems (Zagha and McCormick 2014). More recently, studies have shown that movement is associated with global increases in neocortical activity (Stringer et al. 2019; Musall et al. 2020; Salkoff et al. 2020). As with low activity preceding response trials, we also find that whisker movements are reduced preceding hit trials (Fig. 5), consistent with previous reports (Ollerenshaw et al. 2012; Kyriakatos et al. 2016). We suspect that whisker movements impair detection for multiple reasons: 1) reafference signals from self-generated movements (Fee et al. 1997) may obscure stimulus-evoked afferent signals, 2) self-generated movements may evoke top-down sensory gating and thereby suppress stimulus evoked signals (Chakrabarti and Schwarz 2018), and 3) centrally mediated cortical activation associated with whisker

movements (Poulet et al. 2012) may reduce network excitability. And yet, our findings support a view of cortical state as higher dimensional than stationary versus moving (Zagha and McCormick 2014; McGinley, Vinck, et al. 2015b). Among Hit trials, we find a positive correlation between prestimulus activity and reaction time (Fig. 3). This suggests that even within overt changes in arousal, the precise levels of cortical activity impact performance in our task, with the lowest prestimulus activity correlating with optimal performance.

The neural processes that underlie the low amplitude, low variable widefield Ca^{2+} imaging signals preceding response trials could be due to multiple mechanisms. One possibility is that these low-amplitude signals reflect a "desynchronized" cortical state, as observed in whole-cell recordings, EEG, or LFP signals during wakefulness and high arousal compared to sleep and low arousal (Poulet and Petersen 2008; Tan et al. 2014; Zagha and McCormick 2014). To test this possibility, we analyzed LFP power and spike-triggered average LFP power from three different cortical areas. Overall, these measures did not identify differences in cortical state preceding response versus no response outcomes. A second possibility is that the low-amplitude Ca^{2+} imaging signals reflect low spiking activity. To test this possibility, we analyzed prestimulus spike rates from the same cortical areas as in the LFP analyses. Indeed, we observed significantly reduced spike rates before response compared to no response trials. Thus, the low-amplitude Ca^{2+} imaging signals can, at least in part, be accounted for by reduced spike rates. We do recognize a difference in magnitude: the prestimulus reductions in dF/F are larger than the reductions in spike rate when converted to a common metric (such as *d'*, data not shown). This may simply reflect a sub-sampling of spiking activity. However, a third possibility is that the low-amplitude Ca^{2+} imaging signals reflect robust modulations of apical dendrites, with only modest impacts on axo-somatic spike rates. We suspect that most of the Ca^{2+} imaging signals reported here are derived from the

apical dendrites of supragranular and infragranular pyramidal neurons. Local spikes in these apical dendrites have been shown to modulate axo-somatic spiking output (Branco and Häusser 2011; Smith et al. 2013; Palmer et al. 2014). However, the long electrotonic distances between these compartments indicate the possibility of partial local control; robust prestimulus modulation of apical dendritic excitability may have only minor impacts on axo-somatic spike output, yet greatly impact dendritic integration and plasticity in response to sensory inputs. Recent studies have identified specific dis-inhibitory neural circuits that control the excitability of apical dendrites (Lee et al. 2013; Pi et al. 2013; Fu et al. 2015). Future studies, recording specifically from these interneuron populations, are needed to further assess this possibility.

Supplementary Material

Supplementary material can be found at *Cerebral Cortex* online.

Funding

Notes

References

Andreou C, Borgwardt S. 2020. Structural and functional imaging markers for susceptibility to psychosis. *Mol Psychiatry*. 25(11):2773–2785.

Arieli A, Shoham D, Hildesheim R, Grinvald A. 1995. Coherent spatiotemporal patterns of ongoing activity revealed by real-time optical imaging coupled with single-unit recording in the cat visual cortex. *J Neurophysiol*. 73(5):2072–2093.

Arieli A, Sterkin A, Grinvald A, Aertsen A. 1996. Dynamics of ongoing activity: explanation of the large variability in evoked cortical responses. *Science*. 273(5283):1868–1871.

Aruljothi K, Marrero K, Zhang Z, Zareian B, Zagha E. 2020. Functional localization of an attenuating filter within cortex for a selective detection task in mice. *J Neurosci*. 40(28):5443–5454.

Boly M, Balteau E, Schnakers C, Degueldre C, Moonen G, Luxen A, Phillips C, Peigneux P, Maquet P, Laureys S. 2007. Baseline brain activity fluctuations predict somatosensory perception in humans. *Proc Natl Acad Sci*. 104(29):12187–12192.

Branco T, Häusser M. 2011. Synaptic integration gradients in single cortical pyramidal cell dendrites. *Neuron*. 69(5):885–892.

Britten K, Shadlen M, Newsome W, Movshon J. 1992. The analysis of visual motion: a comparison of neuronal and psychophysical performance. *J Neurosci*. 12(12):4745–4765.

Cardin JA, Palmer LA, Contreras D. 2008. Cellular mechanisms underlying stimulus-dependent gain modulation in primary visual cortex neurons in vivo. *Neuron*. 59(1):150–160.

Chakrabarti S, Schwarz C. 2018. Cortical modulation of sensory flow during active touch in the rat whisker system. *Nat Commun*. 9(1):3907.

Chance FS, Abbott LF, Reyes AD. 2002. Gain modulation from background synaptic input. *Neuron*. 35(4):773–782.

Crochet S, Petersen CC. 2006. Correlating whisker behavior with membrane potential in barrel cortex of awake mice. *Nat Neurosci*. 9(5):608–610.

De Lafuente V, Romo R. 2006. Neural correlate of subjective sensory experience gradually builds up across cortical areas. *Proc Natl Acad Sci*. 103(39):14266–14271.

de Lange FP, Rahnev DA, Donner TH, Lau H. 2013. Prestimulus oscillatory activity over motor cortex reflects perceptual expectations. *J Neurosci*. 33(4):1400–1410.

Fee MS, Mitra PP, Kleinfeld D. 1997. Central versus peripheral determinants of patterned spike activity in rat vibrissa cortex during whisking. *J Neurophysiol*. 78(2):1144–1149.

Ferezou I, Haiss F, Gentet LJ, Aronoff R, Weber B, Petersen CC. 2007. Spatiotemporal dynamics of cortical sensorimotor integration in behaving mice. *Neuron*. 56(5):907–923.

Fiebelkorn IC, Kastner S. 2021. Spike timing in the attention network predicts behavioral outcome prior to target selection. *Neuron*. 109(1):177–188.e4.

Fries P, Reynolds JH, Rorie AE, Desimone R. 2001. Modulation of oscillatory neuronal synchronization by selective visual attention. *Science*. 291(5508):1560–1563.

Fu Y, Kaneko M, Tang Y, Alvarez-Buylla A, Stryker MP. 2015. A cortical disinhibitory circuit for enhancing adult plasticity. *Elife*. 4:e05558.

Ghose GM, Maunsell JH. 2002. Attentional modulation in visual cortex depends on task timing. *Nature*. 419(6907):616–620.

Gold JI, Shadlen MN. 2007. The neural basis of decision making. *Annu Rev Neurosci*. 30:535–574.

Haider B, Duque A, Hasenstaub AR, Yu Y, McCormick DA. 2007. Enhancement of visual responsiveness by spontaneous local network activity in vivo. *J Neurophysiol*. 97(6): 4186–4202.

Haider B, McCormick DA. 2009. Rapid neocortical dynamics: cellular and network mechanisms. *Neuron*. 62(2):171–189.

Hanes DP, Schall JD. 1996. Neural control of voluntary movement initiation. *Science*. 274(5286):427–430.

Harris KD, Thiele A. 2011. Cortical state and attention. *Nat Rev Neurosci*. 12(9):509–523.

Hasenstaub A, Sachdev RNS, McCormick DA. 2007. State changes rapidly modulate cortical neuronal responsiveness. *J Neurosci*. 27(36):9607–9622.

Hô N, Destexhe A. 2000. Synaptic background activity enhances the responsiveness of neocortical pyramidal neurons. *J Neurophysiol*. 84(3):1488–1496.

Kim R, Sejnowski TJ. 2021. Strong inhibitory signaling underlies stable temporal dynamics and working memory in spiking neural networks. *Nat Neurosci*. 24(1):129–139.

Kyriakatos A, Sadashivaiah V, Zhang Y, Motta A, Auffret M, Petersen CCH. 2017. Voltage-sensitive dye imaging of mouse neocortex during a whisker detection task. *Neurophotonics*. 4(3):031204.

Lee S, Kruglikov I, Huang ZJ, Fishell G, Rudy B. 2013. A disinhibitory circuit mediates motor integration in the somatosensory cortex. *Nat Neurosci*. 16(11):1662–1670.

Luck SJ, Chelazzi L, Hillyard SA, Desimone R. 1997. Neural mechanisms of spatial selective attention in areas v1, v2, and v4 of macaque visual cortex. *J Neurophysiol*. 77(1):24–42.

Mazaheri A, DiQuattro NE, Bengson J, Geng JJ. 2011. Pre-stimulus activity predicts the winner of top-down vs. bottom-up attentional selection. *PLoS One*. 6(2):e16243.

McCormick DA, McGinley MJ, Salkoff DB. 2015. Brain state dependent activity in the cortex and thalamus. *Curr Opin Neurobiol*. 31:133–140.

McGinley MJ, David SV, McCormick DA. 2015a. Cortical membrane potential signature of optimal states for sensory signal detection. *Neuron*. 87(1):179–192.

McGinley MJ, Vinck M, Reimer J, Batista-Brito R, Zagha E, Cadwell CR, Tolias AS, Cardin JA, McCormick DA. 2015b. Waking state: rapid variations modulate neural and behavioral responses. *Neuron*. 87(6):1143–1161.

Moore T, Armstrong KM. 2003. Selective gating of visual signals by microstimulation of frontal cortex. *Nature*. 421(6921):370–373.

Murphy MC, Chan KC, Kim SG, Vazquez AL. 2018. Macroscale variation in resting-state neuronal activity and connectivity assessed by simultaneous calcium imaging, hemodynamic imaging and electrophysiology. *Neuroimage*. 169: 352–362.

Musall S, Kaufman MT, Juavinett AL, Gluf S, Churchland AK. 2020. Single-trial neural dynamics are dominated by richly varied movements. *Nat Neurosci*. 22(10):1677–1686.

Niell CM, Stryker MP. 2010. Modulation of visual responses by behavioral state in mouse visual cortex. *Neuron*. 65(4):472–479.

Ollerenshaw DR, Bari BA, Millard DC, Orr LE, Wang Q, Stanley GB. 2012. Detection of tactile inputs in the rat vibrissa pathway. *J Neurophysiol*. 108(2):479–490.

Palmer LM, Shai AS, Reeve JE, Anderson HL, Paulsen O, Larkum ME. 2014. NMDA spikes enhance action potential generation during sensory input. *Nat Neurosci*. 17(3):383–390.

Petersen CCH, Grinvald A, Sakmann B. 2003. Spatiotemporal dynamics of sensory responses in layer 2/3 of rat barrel cortex measured in vivo by voltage-sensitive dye imaging combined with whole-cell voltage recordings and neuron reconstructions. *J Neurosci*. 23(4):1298–1309.

Pi H-J, Hangya B, Kvitsiani D, Sanders JI, Huang ZJ, Kepecs A. 2013. Cortical interneurons that specialize in disinhibitory control. *Nature*. 503(7477):521–524.

Poulet JF, Fernandez LM, Crochet S, Petersen CC. 2012. Thalamic control of cortical states. *Nat Neurosci*. 15(3):370–372.

Poulet JF, Petersen CC. 2008. Internal brain state regulates membrane potential synchrony in barrel cortex of behaving mice. *Nature*. 454(7206):881–885.

Roitman JD, Shadlen MN. 2002. Response of neurons in the lateral intraparietal area during a combined visual discrimination reaction time task. *J Neurosci*. 22(21): 9475–9489.

Rudolph M, Destexhe A. 2003. A fast-conducting, stochastic integrative mode for neocortical neurons in vivo. *J Neurosci*. 23(6):2466–2476.

Sachdev RNS, Ebner FF, Wilson CJ. 2004. Effect of subthreshold up and down states on the whisker-evoked response in somatosensory cortex. *J Neurophysiol*. 92(6):3511–3521.

Sachidhanandam S, Sreenivasan V, Kyriakatos A, Kremer Y, Petersen CCH. 2013. Membrane potential correlates of sensory perception in mouse barrel cortex. *Nat Neurosci*. 16(11):1671–1677.

Salkoff DB, Zagha E, McCarthy E, McCormick DA. 2020. Movement and performance explain widespread cortical activity in a visual detection task. *Cereb Cortex*. 30(1):421–437.

Shimaoka D, Harris KD, Carandini M. 2018. Effects of arousal on mouse sensory cortex depend on modality. *Cell Rep*. 22(12):3160–3167.

Shu Y, Hasenstaub A, Badoual M, Bal T, McCormick DA. 2003. Barrages of synaptic activity control the gain and sensitivity of cortical neurons. *J Neurosci*. 23(32):10388–10401.

Smith SL, Smith IT, Branco T, Häusser M. 2013. Dendritic spikes enhance stimulus selectivity in cortical neurons in vivo. *Nature*. 503(7474):115–120.

Stringer C, Pachitariu M, Steinmetz N, Reddy CB, Carandini M, Harris KD. 2019. Spontaneous behaviors drive multidimensional, brainwide activity. *Science*. 364(6437):255.

Tan AYY, Chen Y, Scholl B, Seidemann E, Priebe NJ. 2014. Sensory stimulation shifts visual cortex from synchronous to asynchronous states. *Nature*. 509(7499):226–229.

van Kempen J, Gieselmann MA, Boyd M, Steinmetz NA, Moore T, Engel TA, Thiele A. 2020. Top-down coordination of local cortical state during selective attention. *Neuron*. 109(5):894–904.e8.

Yang H, Kwon SE, Severson KS, O'Connor DH. 2016. Origins of choice-related activity in mouse somatosensory cortex. *Nat Neurosci*. 19(1):127–134.

Zagha E, McCormick DA. 2014. Neural control of brain state. *Curr Opin Neurobiol*. 29:178–186.

Zareian B, Maboudi K, Daliri MR, Abrishami Moghaddam H, Treue S, Esghaei M. 2020. Attention strengthens across-trial pre-stimulus phase coherence in visual cortex, enhancing stimulus processing. *Sci Rep*. 10(1):4837.

Zareian B, Zhang Z, Zagha E. 2021. Cortical localization of the sensory-motor transformation in a whisker detection task in mice. *eNeuro*. 8(1): ENEURO.0004-21.2021.